Icodahedral short range order in frustrated intermetallic glass

P. Ganesh and M. Widom

Carnegie Mellon University

Department of Physics

Pittsburgh, PA 15213

(Dated: April 26, 2006)

A growing body of experiments display indirect evidence of icosahedral structures in supercooled liquid metals. Computer simulations provide more direct evidence but generally rely on approximate interatomic potentials of unproven accuracy. We use first-principles molecular dynamics simulations to generate realistic atomic configurations, providing structural detail not directly available from experiment, based on interatomic forces that are more reliable than conventional simulations. We analyze the data to quantify the degree of local icosahedral and polytetrahedral order. Comparing elemental metals (Cu **??** and Fe, poor glass formers) we find that the degree of icosahedral order is greater in the BCC Fe as compared to FCC Cu. In Fe-based metallic alloys, (FeB and FeZrB, better glass formers), we find that introduction of a small concentration of small B atoms and large Zr atoms can control the frustration of local icosahedral order.

PACS numbers: 61.43.Dq,61.20.Ja,61.25.Mv

I. INTRODUCTION

Turnbull [1–3] established that metallic liquids can be supercooled if heterogeneous nucleation can be reduced or avoided. Later, Frank [4] showed that icosahedral clustering of 12 atoms about a sphere is energetically preferred to crystalline (e.g. FCC, HCP or BCC) packings for the Lennard-Jones (L-J) pair potentials. The icosahedron is favorable because it is made up entirely of four-atom tetrahedra, the densest-packed cluster possible. Local icosahedral order cannot be propagated throughout space without introducing defects. Based on this, Frank hypothesized that the supercooling of liquid metals might be due to frustrated packing of icosahedral clusters.

Remarkably, the frustration of packing icosahedra is relieved in a curved space, where a perfect 12-coordinated icosahedral packing exists [5–7]. Disclination line defects must be introduced into this icosahedral crystal in order to "flatten" the structure and embed it in ordinary three dimensional space. Owing to the 5-fold rotational symmetry of an icosahedron, the disclination lines are of type $\pm 72°$. The negative disclination line defects that are needed to flatten the structure cause increased coordination numbers of 14, 15 or 16. Large atoms, if present, would naturally assume high coordination number and aid in the formation of a disclination line network.

Many studies of L-J systems have tested Frank's hypothesis. Hoare [8] found that for clusters ranging between 2 to 64 atoms at least three types of "polytetrahedral" noncrystalline structures exist, with a higher binding energy than HCP or FCC structures with the same number of atoms. Honeycutt and Andersen [9] found the crossover cluster size between icosahedral and crystallographic ordering around a cluster size of 5000 atoms. They also introduced a method to count the number of tetrahedra surrounding an interatomic bond. This number is 5 for local icosahedral order. Steinhardt, Nelson and Ronchetti [10] introduced the orientational order parameter $\hat{W}_6$ to demonstrate short range icosahedral order. Jónsson and Anderson [11] observed local five fold symmetry above the glass transition temperature and reported large atoms possess a cluster of interpenetrating and face-sharing icosahedra in a two-component glass.

Many other simulations have been performed on pure elemental metals and metal alloys, using a modified Johnson potential [12], embedded atom potentials [13, 14], the Sutton-Chen (SC) many body potential [15], to name a few. These potentials model the interatomic interactions with varying, and generally uncontrolled, degrees of accuracy. Ab-initio studies on liquid Copper [16–18] and Iron [19] achieve a high degree of realism and accuracy, but have not been analyzed from the perspective of icosahedral ordering.

Undercooling of quasicrystal-forming alloys by electromagnetic levitation [20] suggests that activation energy for formation of quasicrystalline phase nuclei is lower than for crystalline phases. The decrease in activation energy was seen to be more pronounced for the icosahedral phase than for the decagonal phase.

X-ray scattering studies on the deeply undercooled reactive liquid TiZrNi, which has a stable crystalline phase over a wide range of composition, short-range order similar to the liquid and also a metastable quasicrystalline phase, showed correlation between nucleation barrier and a growing icosahedral short range order with decreasing temperature [21]. Neutron scattering studies of deeply undercooled metallic melts [22] observed the characteristic shoulder on the second peak of the structure factor, which has been identified as a signature of icosahedral short range order [23, 24]. The shoulder height increases with decrease in temperature.

A recent XAS experiment on liquid and undercooled liquid Cu by Di Cicco *et al.* [25] isolated the higher order correlation functions. They applied Reverse Monte-Carlo (RMC) refinement [26–28] simultaneously to diffraction and XAS data to construct a model of the disordered system compatible with their experimental data. They analyze the three body angular distribution function N(θ) and also the orientational order parameter $\hat{W}_6$. Their conclusion was that weak local icosahedral order could be observed in their sample. This experiment provided the most direct experimental evidence to-date of the existence of icosahedra in a liquid metal.

Motivated by these results, we explore the structures of liquid and undercooled liquid metals using first principles simulations. First principles calculations achieve the most realistic possible structures, unhindered by the intrinsic inaccuracy of phenomenological potentials and with the ability to accurately capture the chemical nature and distinctions between different elements and alloys. We use the VASP (Vienna Ab-initio Simulation Package [29, 30]) code which solves the quantum mechanical interacting many-body problem using electronic density functional theory. The trade-off for increased accuracy is a decrease in the system sizes we can study, so we can only observe local order, not long range. Also we are limited to short time scales. When we study glassy alloys, we augment our molecular-dynamics simulation with another algorithm called 'Tempering' or 'replica exchange method' (REM) [31, 32] for fast equilibriation at low temperatures.

Our analysis covers methods that have previously been fruitful. We look at the radial distribution function, the three body angular distribution function, which is simply related to the three body correlation function, the $\hat{W}_6$ parameter as discussed above, and the Honeycutt and Andersen bond statistics method [9].

Liquid and supercooled liquid Copper showed only weak icosahedral order and very little temperature variation. On the contrary, Fe showed a monotonic increase in icosahedral order, which became very high, when supercooled. For FeZrB and FeB, we found that FeZrB showed enhanced icosahedral order when supercooled compared to FeB. This could possibly be explained by formation of disclination line defects [23] anchored on the large Zr atoms, which eases the frustration of icosahedral order on the Fe atoms. Analysis of quenched Fe revealed a natural way of forming a single -72° disclination line segment in an otherwise perfect BCC enviroment, without disturbing the entire structure.

We are not aware of a similar construction for FCC. This could explain the high negative $\hat{W}_6$ values observed in supercooled Fe as compared to Cu.

At high temperatures we found that structural properties of liquid Cu and liquid Fe resembled each other closely, and also strongly resembled a maximally random jammed [33] hard sphere configuration. From this we conclude that a nearly universal structure exists for systems whose energetics are dominated by repulsive central forces.

Section II describes our first principles molecular dynamics method in greater detail. Then section III describes the fusion method of monte-carlo and first principles MD, that we will be referring to as 'Tempering MD'.Here we introduce the radial distribution function $g(r)$, the $\hat{W}_6$ bond orientational order parameter, the three body angular distribution function $N(\theta)$, and the Honeycutt and Andersen analysis method. Next, Section IV draws parallels and differences between our Fe and Cu studies. Section **??** repeats this analysis making comparisons between the poor-, moderate- and good-glass-forming series Fe, FeB and FeZrB.

II. FIRST PRINCIPLES METHOD

First principles simulation is an incisive, powerful and well-developed tool based on a quantum mechanical treatment of the electrons responsible for interatomic bonding. Since the method is based on fundamental physical laws and properties of atoms, it can be applied to a wide variety of metal alloys and yields the energy and forces computationally without any adjustable free parameters.

Our $ab-initio$ molecular dynamics simulation program, VASP [29, 30], solves the N-body quantum mechanical interacting electron problem using electronic density functional theory, under the Generalised Gradient Approximation (GGA). We use the ultrasoft pseudopotentials [34, 35] (USPP) or projector-augmented wave [36, 37] (PAW) potentials as provided with VASP. Calculation times grow nearly as the third power of the number of atoms, limiting our studies to sample sizes of around a hundred atoms.

In first-principles molecular dynamics, although interatomic forces and energies are calculated quantum mechanically, we still treat the atomic motions classically, using the Born-Oppenheimer approximation. We use Nose dynamics to simulate in the canonical ensemble at fixed mean temperature. The system was well equilibrated before data was considered for analysis. The simulation started with a random configuration, at a temperature high enough to ensure a liquid state, and was allowed to equilibrate at this high temperature. Subsequently, lower temperatures were simulated starting from previous configurations. All calculations were Γ point calculations (a single 'k' point).

III. TEMPERING MOLECULAR DYNAMICS

Elemental metals crystallise so easily that they can hardly be made amorphous at any given quench rate. Alloying can improve the ease of glass formation. For some special alloys, a bulk amorphous state can be reached by slow cooling. Pure elemental Fe is a poor glass former, but Fe-based compounds like FeB and especially FeZrB, show improved glass formability.

One reason alloys form glass more easily is that chemical identity introduces a new configurational degree of freedom that evolves slowly. Unfortunately, this makes simulation more difficult. It is especially difficult to equilibrate the system at very low temperatures, because the probability to cross an energy barrier drops, trapping in particular configurations for long times. For this reason we use a Monte-Carlo method, known as tempering or replica exchange [31] to augment our first-principles MD. The method we use is similar to the one in reference [32], except they exchange the potential energy scaling parameter, while we exchange the temperature of the different canonical ensembles. This

TABLE I: $\hat{W}_6$ values for a few clusters

Cluster	HCP	FCC	ICOS	BCC
No. of atoms	12	12	12	14
$\hat{W}_6$	-0.012	-0.013	-0.169	+0.013

method allows us to sample the configurational space more efficiently than conventional MD.

In the canonical ensemble, energy fluctuates at fixed temperature. A given configuration C with energy E can occur at any temperature T with probability $e^{-\beta E}$,($\beta = 1/kT$). Now consider a pair of configurations, C_1 and C_2 of energy E_1 and E_2 occurring in simulations, at temperatures T_1 and T_2. We can take C_1 as a member of the ensemble at T_2, and C_2 as a member of the ensemble at T_1, with a probability

$$P = e^{-(\beta_2-\beta_1)(E_1-E_2)} \tag{1}$$

In practice we perform several MD simulations at temperatures separated by 100K. Every 10 MD steps we compare the configurations at two nearby temperatures and swap them with the above probability. As a result, configurations initially frozen at low temperature can have their temperature rise. The simulations then can carry the structure over energy barriers after which the temperature can again drop.

IV. SIMULATION DETAILS

In an effort to explore the structures of compounds with differing glass-forming ability we compare pure elemental Iron and two Iron-based glass-forming alloys. The presence of additional chemical species can enhance glass forming ability owing to the new compositional degrees of freedom. Unfortunately this degree of freedom increases the demands

TABLE II: Details of Tempering MD runs.

Chemical Species	Temperatures(K)	density (Å^{-3})	time (ps)
Fe_{100}	800-1900	0.0756	1.5
$Fe_{80}B_{20}$	800-1500	0.0814	1.8
$Fe_{70}Zr_{10}B_{20}$	800-1800	0.0787	1.8

on simulation because of its slow evolution. Consequently we performed tempering MD, details of the runs are in Table II.

Our simulations must be performed at fixed volume, but we have no rigorous means of predicting the density at high temperature. For pure liquid Iron, the density is known experimentally [38], and we use this value. For FeB and FeZrB, we took a high temperature liquid structure and quenched it, relaxing positions and cell lattice parameters, to find a predicted low temperature density. We then decreased the density of the relaxed structure by 6 percent to account for volume expansion, to arrive at the densities for our liquid simulations. Notice that we hold the volumes constant independent of temperature because our tempering method requires this.

All runs used an MD time step of 2 fs, and reached total simulated time of order 2 ps. During this run time, we saw frequent swapping of configurations at adjacent temperatures, enabling configurations at lower temperatures to spend some time at a higher temperature before they come back to the lower temperature again.

We believe this method explores configuration space rather efficiently, because when applied to pure elemental Fe (and Cu) our structures crystallized rapidly at low temperature. Because of the efficient sampling of our tempering MD method, the structure of pure Fe partially crystallizes at low temperature after about 1 ps. In the following discussion of our T=800K sample we will refer to different structural features before and after crystallization. We also performed conventional MD at T=800K yielding results similar to tempering MD prior to crystallization.

For all Iron-based runs we employed spin polarization, reasoning that local magnetic moments exist even above the Curie point. These local moments have a significant influence on the short-range order because ferromagnetic Iron prefers a longer bond length than antiferromangetic Iron. Of course, the ferromagnetic state of the liquid implies improper long-range correlations. Unfortunately, since our forces are calculated for electronic ground states, we cannot model the true paramagnetic state of liquid Iron and Iron-based alloys.

The following sections explore the impact of alloying on geometry, observing that addition of small Boron atoms greatly reduces the degree of icosahedral structure because they tend to cause +72° disclinations, while large Zirconium atoms partially restore it by stabilizing -72° disclinations.

V. RESULTS

A. Radial Distribution Function $g(r)$

The radial distribution function, $g(r)$, is propoortioal to the density of atoms at a distance r from another atom. We calculate $g(r)$ by forming a histogram of bond lengths using the repeated image method to obtain the bond lengths greater than half the box size. We then smooth out the histogram with a gaussian of standard deviation 0.05Å.

To evaluate the role of magnetism, Fig. 1 illustrates the pair correlation functions for liquid Fe simulated at T=1800K, just below melting (T_m=1833K). Evidentally, the simulation with magnetism yields good agreement in the position and height of the first peak in $g(r)$, while neglect of magnetic moments results in near neighbor bonds that are too short and too weak. However, magnetism overestimates the strength of long-range correlations beyond

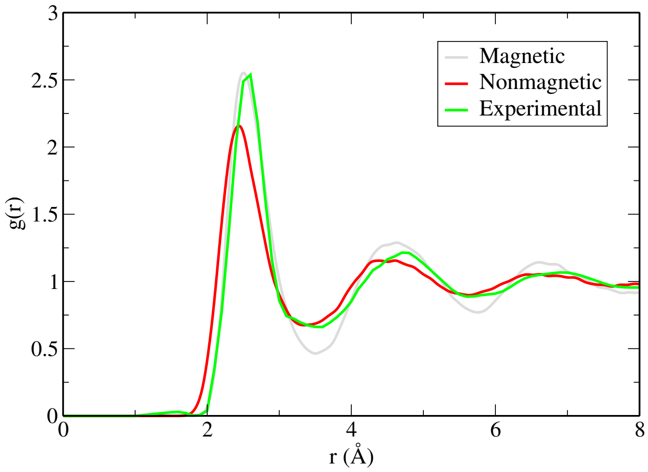

FIG. 1: Pair correlation function of pure elemental liquid Fe. Simulations (magnetic and nonmagnetic) are run at T=1800K, compared with experiment at T=1833K.

the nearest-neighbor peak. Neverthless, for the present study of local order, it is necessary to make spin polarised calculations.

Table III shows the details of the different pair correlation functions, in supercooled FeZrB at T=800K. From the heights of the first peak in FeZrB, we see that the strongest bonds form between B and Fe and between B and Zr. Also, the relative bond lengths reveal that B is a small atom, Fe is medium sized and Zr is large. Comparing with simulations of FeB and pure Fe, we find that g_{FeFe} is reduced by alloying with B or ZrB, since the fraction of Fe atoms have reduced in the sample. We also notice that the peak height is slightly more in the presence of Zr. This could be because in FeB the centers of disclination were Fe while in FeZrB we have many disclinations with Zr centers, pitching the Fe atoms closer. g_{FeB} and g_{BB} are nearly unaffected by alloying with Zr.

B. Bond Orientation Order Parameter $\hat{W}_6$

Next we examine the $\hat{W}_6$ distribution. For pure Fe, at high temperatures it resembles that of high temperature liquid Cu, which in turn resembles the maximally random jammed configuration of hard spheres. However, as temperature drops the $\hat{W}_6$ distribution shifts strongly to the left, resulting in rather high concentrations of nearly icosahedral clusters as shown in Fig. 2 before crystallization.

We checked the $\hat{W}_6$ distribution of a nonmagnetic simulation to see if it is strongly influenced by magnetism, and found a nearly identical result. In particular, we still found a strong enhancement of the nearly icosahedral clusters relative to liquid Cu.

To inspect the origin of this low $\hat{W}_6$ peak, we performed a voronoi analysis [39] of the liquid before crystallization. A Voronoi polyhedron is described by indices as $(F_3, F_4, F_5, ...)$ where F_i denotes the number of faces with i edges. For example (0,0,12) denotes an icosahedron, while (0,0,12,2) denotes a 14-coordinated (Z14) atom, with 12 5-fold bonds and 2 6-fold bonds. This is a characteristic TCP structure of the Frank-Kasper type, with a -72° disclination line running through an otherwise perfect icosahedron. In a body-centered cubic crystal all atoms are of Voronoi type (0,6,0,8), which is an alternate 14-coordinated structure.

The T=800K liquid before crystallization contains on average 12% of atoms with Voronoi type (0,0,12) and 3% of atoms of type (0,0,12,2). The Z14 atoms tended to be near-neighbors, linked along their 6-fold (-72°) bonds. After crystallization these percentages drop to 6% and 2% respectively. Supercooled Cu in contrast contains about 1% of (0,0,12) and no (0,0,12,2). The MRJ configuration contains 3% (0,0,12) but no (0,0,12,2).

After crystalization, the distribution at T=800K was strongly peaked around $\hat{W}_6 = 0$, consistent with the value

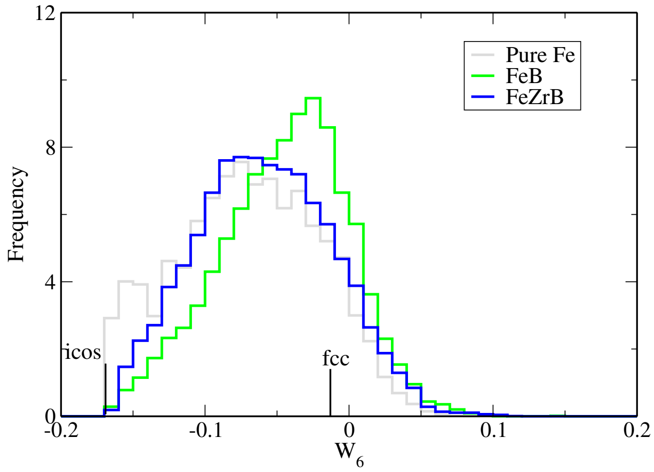

FIG. 2: Distribution of $\hat{W}_6$ around Fe atoms, in supercooled Fe, FeB and FeZrB at T=800K

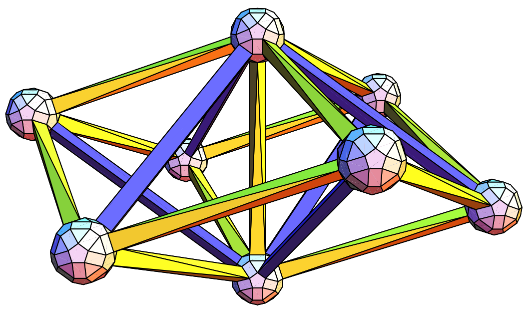

FIG. 3: Fragment of BCC crystal illustrating central bond in the [1,1,1] (vertical) direction surrounded by two equilateral triangles. Displacing these atoms to their midplane and rotating 30° converts the central bond into a -72° disclination line defect. Balls and sticks follow ZomeTool convention: Balls are icosahedral, yellow sticks are 3-fold and blue sticks are 2-fold bonds.

for ordinary crystalline clusters, but retaining a subset of atoms with nearly icosahedral $\hat{W}_6$<-0.14. Not suprisingly, these were precisely the atoms of Voronoi type (0,0,12).

To understand the presence of icosahedral structure in our partially crystallized sample, we quenched this structure by conjugate gradient relaxation of atomic coordinates and lattice parameters. After relaxation we found 56 atoms had BCC Voronoi type (0,6,0,8). The 6 icosahedral atoms became 12-coordinated (0,4,8) structures surrounding the 2 (0,0,12,2) disclinated icosahedral atoms, which retained their type. The remaining atoms served to link the cluster of icosahedron-related atoms to the surrounding defect-free crystal.

The icosahedron-related structure thus forms a point defect in an otherwise perfect BCC crystal. A simple way to create this defect is to take two consecutive triangles surrounding a near-neighbor bond along the BCC [1,1,1] direction (see Fig. 3), displace them into the perpendicular bisecting plane and rotate by 30°. The atoms along the [1,1,1] bond become (0,0,12,2)'s and the six surrounding atoms become (0,4,8)'s. We compared the energy of a crystal containing this defect to perfect BCC Iron and found the energy cost of the defect was 5.3 eV.

Embedding an icosahedral structure into a BCC crystal is quite natural, because a BCC structure can be built up from objects of icosahedral symmetry linked along their axes of 2- and 3-fold rotational symmetry, as is indeed illustrated in Fig. 3. This is not possible for FCC. Since tungsten, W, also crystallises in BCC, we performed a seperate first-principles simulation of liquid tungsten. After supercooling W by 13% to T=3200K we found the $\hat{W}_6$ histogram resembled that of Fe at 1600K (which is 15% supercooled). A voronoi analysis revealed a similar percentage of (0,0,12)'s and (0,0,12,2)'s in both these elemental BCC metals.

We believe the relationship between BCC and icosahedral structures may be linked to our observed high fraction of icosahedra in liquid Fe as compared to Cu.

To define the $\hat{W}_6$ distribution in an alloy, we concentrate on central atoms of some particular species (e.g. Fe) but consider the neighboring atoms of all species. To calculate the $\hat{W}_6$ distributions for Fe, FeB, and FeZrB alloys we chose the near-neighbor cutoff distances near the first minima of the partial pair correlation functions (Table III).

Compare the Fe-based $\hat{W}_6$ distributions at their supercooled temperatures in Fig. 2. The FeB distribution is similar

TABLE III: R_{peak}, $g(R_{peak})$ and R_{min} for FeZrB at T=800K

chemical pairs	Fe-Fe	Fe-Zr	Fe-B	Zr-Zr	Zr-B	B-B
R_{peak}(Å)	2.57	2.90	2.14	3.44	2.61	1.75
$g(R_{peak})$	3.05	3.38	4.5	1.42	4.57	1.76
R_{min}(Å)	3.50	3.83	2.99	4.06	3.31	2.37

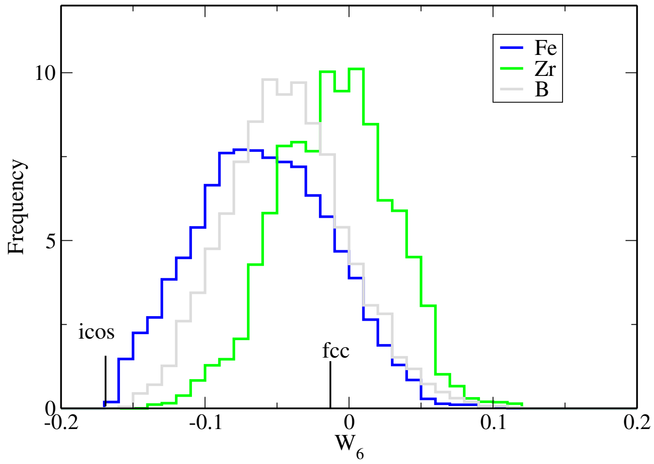

FIG. 4: Distribution of $\hat{W}_6$ for different chemical species in supercooled FeZrB at T=800K

to high temperatures, but the FeZrB curve has significantly shifted to the left, extending more towards the ideal icosahedral value of $\hat{W}_6$. The origin of high negative $\hat{W}_6$ values for pure Fe has been explained in section IV

At temperatures as low as T=800K, the energy of the system is close to the lowest configurational energy of the system, and locally, an icosahedral configuration has the lowest energy. Replacing a few medium sized Fe atoms with smaller B atoms would cause disclination lines to concentrate on Fe, leading to a distortion from ideal icosahedral clustering on these Fe atoms. This causes a reduction in the extreme negative values of $\hat{W}_6$ on Fe atoms in FeB. On the contrary, inclusion of Zr in FeZrB causes disclinations to attach to Zr, easing frustration leading to more Fe

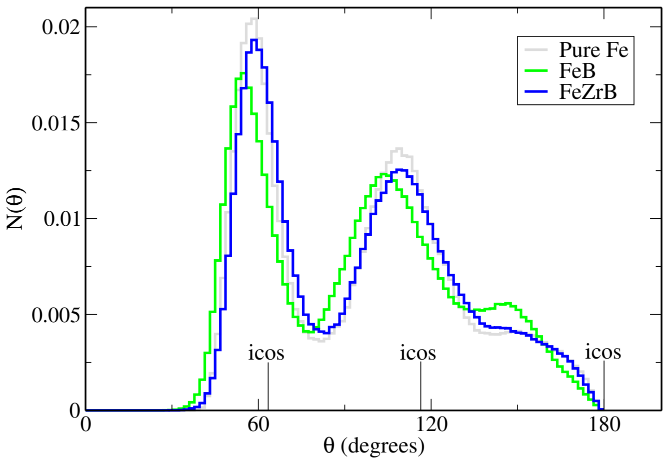

FIG. 5: Distribution of N(θ) for Fe in Pure Fe, FeB and FeZrB at T=800K

centered clusters with icosahedral ordering. This causes an increase in the negative region of $\hat{W}_6$, as compared to FeB. So it seems that inclusion of the big Zr atom tends to make the local 3D structure around the Fe atoms, more nearly icosahedral. The shift towards the ideal icosahedron value, in the $\hat{W}_6$distribution of FeZrB, suggests that alloying of FeB with the large Zr atom increases icosahedral ordering.

Fig 4 shows the distribution with centers at Fe, Zr and B, for FeZrB. The histogram with the center at Zr is almost symmetric about the value of zero. This suggests that the local environment about Zr atoms is nearly spherical, as is expected given its large size. The B centered $\hat{W}_6$ histogram is also assymmetric towards negative $\hat{W}_6$ values, and doesn't show any significant change between the two supercooled alloys. Both the B based and Zr based histograms don't show any dramatic change with lowering of temperature or with alloying.

C. Bond-Angle Distribution N(θ)

The three body angular distribution was calculated for the configurations at different temperatures. As in the case of $\hat{W}_6$, we concentrate on central atoms of some particular species but consider the neighboring atoms of all species. The cutoff for the calculation of the angular distribution was taken near the first minima of the partial $g(r)$. Fig 5 shows the angular distribution, centered on Fe. In each case, there are sharp peaks around values of 60° and 110°, and a minimum at 90°. The minima at 90° shows that there isn't any cubic order in the system. The peaks at 60°, show that there are many nearly equilateral triangles indicating tetrahedral order, which could have come from icosahedrons. The height at these two peak positions, is more for FeZrB than for FeB at 800K. This again supports the idea of getting more icosahedra by the inclusion of larger Zr atoms. We also notice that these peaks in FeZrB have become higher with supercooling, unlike in FeB. This also supports our conclusion from the $\hat{W}_6$ distribution, that Zr atoms tend to increase icosahedral order on supercooling, easing the process of supercooling of the alloy. That is, it is easier to supercool FeZrB than FeB. The observation, that pure Fe also has the same height as that of FeZrB supports the observation in section IV. Also notice, that addition of ZrB to Fe, probably has reduced the melting point of FeZrB below that of pure Fe, so that at T=800K pure Fe is supercooled to a higher percentage than the alloys. The Fe sample crystallized after a while at T=800K, while the FeZrB didn't crystallize. The increasing icosahedral order in FeZrB with supercooling would then suggest that it is probably possible to supercool FeZrB to temperatures below 800K. We again see a broad maximum from 150°. This may be due to the flattening of the ideal icosahedron peak at the extremum value of 180°.

The angular distribution of B (not shown here), shows peaks at 70° and 128° with a minima at 97°. The position

TABLE IV: HA analysis for supercooled FeZrB at T=800K

chemical species	Fe-Fe	Fe-Zr	Fe-B	Zr-Zr	Zr-B	B-B
14 pairs	0.30	0.19	0.54	0.11	0.55	0.75
15 pairs	0.56	0.53	0.39	0.48	0.41	0.18
16 pairs	0.10	0.24	0.01	0.36	0.01	0.01

of the peak heights are shifted by about 7-12 degrees to the right, as compared to the ideal icosahedron peaks. This may be due to the small size of the B atoms, which naturally will tend to increase angles of bonds they form with large atoms. Similarly, peaks on Zr based N(θ) (not shown here) lie around 55° and 96°, about the same values taken by a Friauf polyhedra with a coordination number of 16 [40]

D. Honeycutt and Andersen analysis

HA statistics show tetrahedral and polytetrahedral ordering. Tetrahedral order supports icosahedral ordering. A Honeycutt and Andersen analysis for pure Fe, with an R_{cut}=3.4Å, showed that with supercooling the fraction of "5" bonds rises from 0.40 at T=1900K to 0.56 at T=800K in the liquid before crystallization, while the fraction of "4" bonds drops from 0.40 to 0.30. The fraction of "6" bonds remains nearly constant at 0.07. After crystallization at the lowest temperature of T=800K, the "5" bonds decrease to 0.50 while the "4" bonds increase to 0.40. The "6" bonds also show a slight increase to 0.09.

Since FeZrB showed maximal icosahedral clustering when supercooled, as compared to FeB, we made a HA analysis to the ternary glassy alloys, by looking at pairs of chemical species. The vale of the R_{cut} has been chosen in a manner similar to the $\hat{W}_6$ analysis. The frequency has been normalised such that the $1x$ pairs show the fraction of bonded pairs of that particular chemical species. Table IV lists the fraction of different $1x$ pairs in supercooled FeZrB.

Among the $1x$ pairs, with Fe as one of the root pairs, the "15"'s are most abundant at all temperatures. They also show a steady enhancement with supercooling, unlike the "14"'s which decrease with supercooling. The percentage of "15"'s for each of the Fe pairs is about the same for both the alloys at all temperatures, as also for pure Fe. Supercooled pure Fe has very few "16"'s (7%), about the same as in pure Cu. Adding B to Fe, shows an increase of "16"'s for Fe-Fe pairs to 21%. So additions of a few B atoms, leads to many Z16, Fe centers, making the local geometry about the Fe atoms more spherical. That is why we see the Fe centered $\hat{W}_6$ in FeB shift towards more positive values. Further inclusion of large Zr atoms to FeB, decreases the "16"'s about the Fe-Fe pairs, easing the frustration off Fe centers. This causes the geometry about Fe centers to be more icosahedral, and hence the shift of the $\hat{W}_6$ towards negative values.

VI. CONCLUSION

This study quantifies icosahedral and polytetrahedral order in supercooled liquid metals and alloys. This is the first such analysis of glass forming Fe compounds, using configurations from first-principles simulations. While the structural properties of Fe and Cu strongly resemble each other at high temperature, and indeed are close to a maximally random jammed structure [33], their behavior evolves substantially, and in different manners, as the liquid is supercooled. Proper modeling of atomic interactions is essential to capture the differing behavior of each element, and use of a first-principles simulation is the most reliable means of achieving this.

For pure elements we find the degree of local icosahedral order in the supercooled liquid depends on the low temperature crystal structure, with BCC metals such as Fe accomodating icosahedra more readily than FCC elements such as Cu. Alloying with large or small atoms can further influence the degree of icosahedral order, with small atoms (e.g. B in Fe) aggravating the frustration by introducing positive disclination line defects, while large atoms (e.g. Zr in Fe) naturally stabilize negative discliation line defects, relieving frustration. We suggest that the formation of icosahedral order and disclination line network, together with the slow dynamics of chemical ordering in an alloy, enhances the glass-forming ability of FeZrB compared with pure Fe or FeB.

Acknowledgments

This work was supported in part by DARPA/ONR grant N00014-01-1-0961. We thank Sal Torquato for providing Maximally Random Jammed (MRJ) configurations.

[1] D. Turnbull, J. Appl. Phys. **21**, 1022 (1950).

[2] D. Turnbull, J. Metals **188**, 1144 (1950).

[3] D. Turnbull and R. E. Cech, J. Appl. Phys. **21**, 804 (1950).

[4] F. C. Frank, Proc. R. Soc. London A **215**, 43 (1952).

[5] J. F. Sadoc and R. Mosseri, Phil. Mag. B **45**, 467 (1982).

[6] D. R. Nelson, Phys. Rev. Lett. **50**, 92 (1983).

[7] J. P. Sethna, Phys. Rev. Lett. **51**, 2198 (1983).

[8] M. R. Hoare, J. Cryst. Growth **17**, 77 (1972).

[9] J. D. Honeycutt and H. C. Andersen, J. Phys. Chem. **91**, 4950 (1987).

[10] P. J. Steinhardt, D. R. Nelson, and M. Ronchetti, Phys. Rev. B **28**, 784 (1983).

[11] H. Jónsson and H. C. Andersen, Phys. Rev. Lett. **60**, 2295 (1988).

[12] T. Tomida and T. Egami, Phys. Rev. B **52**, 3290 (1995).

[13] C. Kuiying, L. Hongbo, L. Xiaoping, H. Quiyong, and H. Zhuangqi, J. Phys. Condens. Matter **7**, 2379 (1995).

[14] B. Sadigh and G. Grimvall, Phys. Rev. B **54**, 15742 (1996).

[15] H. J. Lee, T. Cagin, W. L. Johnson, and W. A. Goddard, J. Chem. Phys. **119**, 9858 (2003).

[16] A. Pasquarello, K. Laasonen, R. Car, C. Lee, and D. Vanderbilt, Phys. Rev. Letts. **69**, 1982 (1992).

[17] G. Kresse and J. Hafner, Phys. Rev. B **48**, 13115 (1993).

[18] A. A. Valladares, To be published (????).

[19] D. Alfe, G. Kresse, and M. J. Gillan, Phys. Rev. B **61**, 132 (2000).

[20] D. Holland-Moritz, D. M. Herlach, and K. Urban, Phys. Rev. Lett. **71**, 1196 (1993).

[21] K. F. Kelton et al., Phys. Rev. Lett. **90**, 195504 (2003).

[22] T. Schenk, D. Holland-Moritz, V. Simonet, R. Bellisent, and D. M. Herlach, Phys. Rev. Lett. **89**, 075507 (2002).

[23] D. R. Nelson and M. Widom, Nucl. Phys. B **240**, 113 (1984).

[24] S. Sachdev and D. R. Nelson, Phys. Rev. Lett. **53**, 1947 (1984).

[25] A. D. Cicco, A. Trapananti, and S. Faggioni, Phys. Rev. Lett. **91**, 135505 (2003).

[26] R. L. McGreevy, J. Phys. Condens. Matter **13**, R877 (2001).

[27] S. J. Gurman and R. L. McGreevy, J. Phys. Condens. Matter **2**, 9463 (1990).

[28] Y. Wang, K. Lu, and C. Li, Phys. Rev. Lett. **79**, 3664 (1997).

[29] G. Kresse and J. Hafner, Phys. Rev. B **47**, RC558 (1993).

[30] G. Kresse and J. Furthmuller, Phys. Rev. B **54**, 11169 (1996).

[31] R. H. Swendsen and J. S. Wang, Phys. Rev. Lett. **57**, 2607 (1986).

[32] R. Yamamoto and W. Kob, Phys. Rev. E **61**, 5473 (2000).

[33] S. Torquato, T. M. Truskett, and P. G. Debenedetti, Phys. Rev. Lett. **84**, 2064 (2000).

[34] D. Vanderbilt, Phys. Rev. B **41**, 7892 (1990).

[35] G. Kresse and J. Hafner, J. Phys. Condens. Matter **6**, 8245 (1994).

[36] P. Blochl, Phys. Rev. B **50**, 17953 (1994).

[37] G. Kresse and D. Joubert, Phys. Rev. B **59**, 1758 (1999).

[38] Y. Waseda, The Structure of Non-Crystalline Materials (1980), (McGraw-Hill, New York).

[39] J. L. Finney, Proc. R. Soc. A **319**, 479 (1970).

[40] J. Hafner, J. Phys. F: Met. Phys. **18**, 153 (1988).